Hindawi
International Journal of Aerospace Engineering
Volume 2022, Article ID 9647206, 19 pages
https://doi.org/10.1155/2022/9647206

Research Article

Numerical Investigation of an Unsteady Blade Surface Blowing Method to Reduce Rotor Blade-Vortex Interaction Noise

Yan Sun, Guohua Xu, and Yongjie Shi

National Key Laboratory of Rotorcraft Aeromechanics, Nanjing University of Aeronautics and Astronautics, Nanjing, Jiangsu 210016, China

Correspondence should be addressed to Guohua Xu; ghxu@nuaa.edu.cn

Received 21 December 2021; Revised 6 July 2022; Accepted 2 August 2022; Published 27 August 2022

Academic Editor: Dakun Sun

This paper presents a numerical investigation of unsteady surface blowing using periodic variations of jet velocity with azimuthal angle to reduce helicopter rotor blade-vortex interaction (BVI) noise. The unsteady blowing is modeled as the mass flow outlet boundary condition of time-varying jet velocity on the blade surface grid using computational fluid dynamics. The same high-resolution overset grid system and flow/noise solver are used to perform a detailed flow field simulation and noise prediction for the nonblowing baseline case and the steady/unsteady blowing cases under the rotor BVI condition, and a grid convergence study for the steady and unsteady blowing cases is carried out. The BVI noise reduction and rotor thrust coefficient results of the unsteady blowing method and the previously published steady blowing with constant jet velocity are then compared. The noise reduction level of unsteady blowing is approximately equivalent to that of steady blowing (noise reduction is more than 3 dB). However, the loss in rotor thrust coefficient caused by unsteady blowing (3.3%) is only half of that by steady blowing (6.3%); the air mass cost by unsteady blowing is only 63.7% of that by steady blowing per rotation revolution. The results show that unsteady blowing can effectively reduce BVI noise with lower cost and less thrust loss.

1. Introduction

Reducing rotor blade-vortex interaction (BVI) noise to combat helicopter noise pollution has become an increasingly urgent task in helicopter aerodynamics and aeroacoustics [1, 2]. BVI is the phenomenon in which the tip vortex trailing from the rotor tip directly strikes with the following blades during low-speed descending flight or maneuvers, resulting in strong fluctuations in the aerodynamic load on the blade surface. This process causes significant BVI noise, which is essentially a kind of vortex-induced aerodynamic noise [3, 4]. The studies in tip vortex formation, evolution, and vortex dynamics have been an increasingly active research field [5–10]. And many researchers [11–13] have employed flow control methods in the tip vortex to reduce BVI noise, specifically to control the structure, strength, and trajectory of the tip vortex.

As an active vortex control method, rotor tip air mass injection (TAMI) technology [13] works by arranging jet ducts at the rotor tip or on the blade surface to blow out compressed air, which can increase the diffusion, reduce the strength, or alter the trajectory of the tip vortex, thereby reducing BVI noise. This active control concept based on positive mass jet blowing on the blade surface has successfully demonstrated an excellent ability to control the tip vortex structure and trajectory in many experiments and numerical studies [14–16]. However, previous research results on blade surface blowing have illustrated that blowing will have an adverse effect on rotor aerodynamics and may cause a significant loss in the rotor thrust [17–19]. This phenomenon of rotor thrust loss caused by surface blowing has not been thoroughly considered in previous studies. Liu et al. [17] investigated the effectiveness of upper surface blowing to alter the tip vortex strength of a hovering rotor. However, in this research, surface blowing caused a thrust loss of up to 29.4% compared with the nonblowing case. Duraisamy and Baeder [18, 19] studied the effect of steady spanwise and streamwise blowing on the tip vortex structure of a single-blade hovering rotor. The blowing significantly

reduced the swirl velocity and the strength of the tip vortex but resulted in a maximum of 6.5% loss in the rotor thrust. The authors of this paper [20, 21] previously conducted a parametric analysis of the effects of the jet slot location on the blade surface, jet velocity, and jet slot area of the steady blowing to reduce the rotor BVI noise and found that there was an optimal steady blowing jet velocity that could achieve a maximum noise reduction of 3.6 dB with the minimum thrust loss of 6.3%. Since rotor design is a complex multidisciplinary program, the design goal of a low-noise rotor is often constrained by aeroacoustics, aerodynamics, aeroelastic stability, and even vibration problems [22]. Achieving noise reduction through a significant sacrifice in the rotor thrust is unacceptable in actual blade design [2], which is also an obstacle restricting the practical application of TAMI technology. Therefore, we attempt to further reduce BVI noise with minimal loss in rotor thrust in this work.

In addition to the work based on the steady blowing discussed above, researchers are also increasing interest in the application of unsteady blowing concepts. Vasilescu and Dancila [23–25] carried out research on the effects of a tangential unsteady spanwise blade tip blowing on the formation and evolution mechanism of the rotor tip vortex in hover, where the air mass flow rate of the unsteady blowing was periodically modulated by changing the jet slot area using a piezoelectrically actuated servo valve. The results in their study showed that unsteady blowing was more efficient for vortex diffusion than steady blowing. The reduction of vortex strength of the unsteady blowing reached the same level as that of steady blowing, where the average blowing cost was two times lower than the average blowing cost of steady blowing. Few studies have been conducted on BVI noise reduction using unsteady blowing. Considering that unsteady blowing may have better application potential than steady blowing, based on the previous work [20, 21] we have carried out on the mechanism and parametric analysis of steady surface blowing on BVI noise reduction, there is significant research motivation to investigate the reduction of rotor BVI noise using unsteady blowing control.

In this paper, a new unsteady blade surface blowing method is proposed in which the jet velocity changes periodically with the rotor azimuthal angle. The compressible unsteady Reynolds-averaged Navier-Stokes (URANS) equations with the improved fifth-order weighted essentially nonoscillatory (WENO-Z) scheme and Farassat's Formulation 1A based on the Ffowcs Williams–Hawkings (FW-H) equations are used to investigate the effect of the unsteady blowing on the blade surface to reduce rotor BVI noise. The unsteady blowing is modeled by the established mass flow outlet boundary conditions on the blade surface grid by modifying the velocity term of the flux in the URANS equations. The high-resolution overset grid system and the flow/noise solver are used to compare the rotor flow field simulation and noise prediction results of the nonblowing baseline case and steady/unsteady blowing cases under the rotor BVI condition.

The remainder of this paper is organized as follows. Section 2 provides a brief overview of the computational method, including the description of the grid system, the introduction of the flow solver and the noise solver, and the modeling of the unsteady blowing. In Section 3, the grid convergence of steady and unsteady blowing cases is studied. The changes in the rotor flow field and the BVI noise results of the unsteady blowing case are discussed and compared with the nonblowing baseline case and the steady blowing case. The effects on the rotor thrust coefficient are also analyzed in detail. Finally, the main conclusions of this paper are summarized in Section 4.

2. Computational Methodology

2.1. Grid System. The grid system used in the computations consists of two body-fitted blade grids with C-O topology and a Cartesian background grid. The moving overset grid method is used to simulate the rotation, pitching, and flapping of the rotor blade motion. As shown in Figure 1, the rotor hub serves as the origin of the coordinate system, and the incoming stream direction is the $+x$-axis, where the $+x$-axis points to the rotor 0° azimuthal angle. The inflow and outflow boundary conditions are imposed on the outer boundary of the background grid in the x-direction. The $+y$-axis points below the rotor plane, and the $+z$-axis points to the 90° azimuthal angle. The normal distance from the wall to the outer boundary of the airfoil is 2 c (chord length). The key issue for accurately predicting BVI noise is to capture the flow details of the wake system for the study of the BVI phenomenon. To improve the resolution of the wake capture, the grid points in the normal direction of the two-dimensional airfoil grid and the grid points in the spanwise direction near the region of the tip vortex core of the three-dimensional blade grid are thoroughly refined, and about 40 grid points cross through the vortex core. As described in our previous work [20, 21], to simulate surface blowing, about 15 grid points are uniformly refined at the 92–95% radius of the blade in the spanwise direction, which is used to define the jet slot on the blade surface. The points of the single blade grid used are $225 \times 80 \times 155$ (corresponding to the blade streamwise, normal, and spanwise directions, respectively). The background grid is a cube-shaped Cartesian grid with the outer boundary length of 7 R (rotor radius), 5.5 R, and 6 R (corresponding to the x-, y-, and z-directions, respectively), and the finest grid spacing in the background grid is 0.1 c (chord lengths). The background grid uses $300 \times 166 \times 247$ points. Our previous study [20] showed that the background grid resolution had a great effect on the rotor wake simulation and BVI noise prediction. Therefore, two more background grid resolutions [20] based on the mentioned $300 \times 166 \times 247$ background grid are employed in the grid convergence study for the steady/unsteady blowing cases. The finer background grid uses $300 \times 331 \times 247$ points with twice the number of the points in the y-direction. The coarser background grid uses half of the grid points in the y-direction, with the grid points of $300 \times 83 \times 247$. These three kinds of background grids are the ones we used for the grid convergence study in [20], but in that research, we only evaluated the grid convergence for the nonblowing case. This paper will revisit the grid

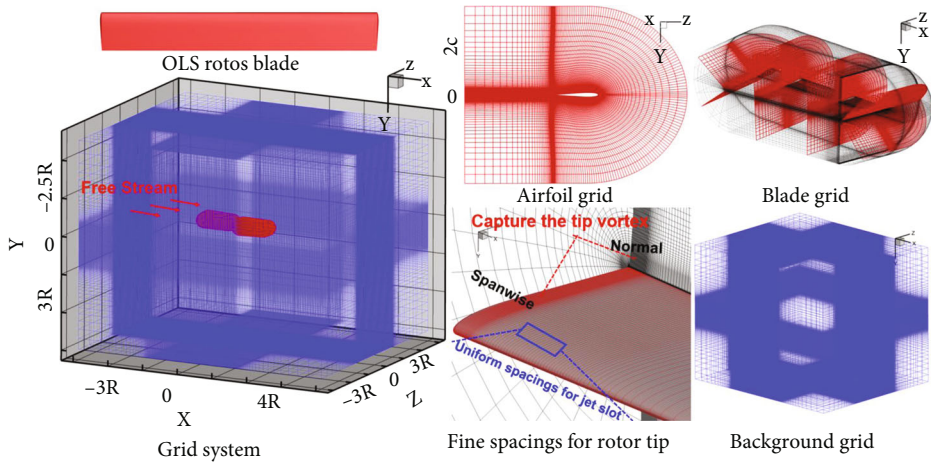

Figure 1: Grid system used for the nonblowing baseline case and the blowing cases.

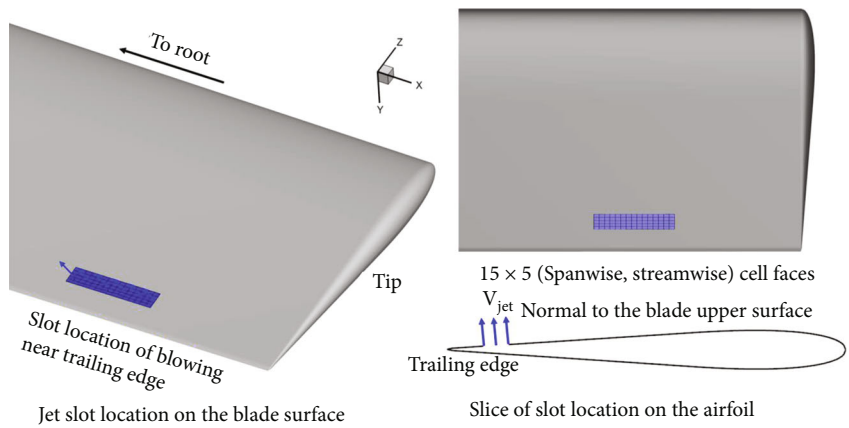

Figure 2: Blowing jet slot location on the blade surface.

convergence study for the steady and unsteady blowing cases. The three grid resolutions use the same two 225 × 80 × 155 blade grids. Here, we refer to these three grid resolutions as Benchmark Grid, Finer Grid, and Coarser Grid, respectively, for distinction.

2.2. Flow Solver. The flow field simulation of the rotor BVI uses the rotor computational fluid dynamics (CFD) codes that have been developed by our research group over many years. The self-programming CFD codes have a wide range of applications in the simulation of single/coaxial rotor hovering and forward flight [10, 20, 21, 26, 27], with good accuracy and robustness. The specific introduction of the flow solver has been previously studied in detail [20]. The URANS equations in the inertial coordinate system are used as the governing equations, and the finite-volume method is used to spatially discretize the governing equations. The computation of the inviscid terms adopts the Roe flux-difference splitting scheme, and the flux variables on the left and right sides of the interface are reconstructed by the fifth-order WENO-Z scheme [28]. The viscous term is computed by the second-order central difference scheme. The dual time-stepping iterative method is used for time advance, and the pseudotime stepping is calculated by the implicit lower-upper symmetric Gauss–Seidel (LU-SGS) scheme. The Spalart–Allmaras (S-A) one-equation turbulence model is adopted to simulate the effects of turbulence in this work.

2.3. Noise Solver. The noise solver has also been previously described in detail [20, 29]. Thus, we briefly introduce the noise computational method here. The self-programming codes for predicting rotor aerodynamic noise are developed according to Farassat's Formulation 1A [30, 31] based on the FW-H equation acoustic analogy, which provides clear physical insight. The blade surface is selected as the integral surface, and the acoustic pressure is the sum of the acoustic pressure due to thickness and loading. After the flow solver computation is completed, the grid coordinates and the pressure of the blade surface grid points output by the CFD codes are used as the input of the acoustic codes for the noise prediction, and the noise information at the observer position can be obtained by integrating Formulation 1A at the retarded time.

2.4. Unsteady Blowing Model. As mentioned in our earlier work [20, 21], the surface blowing model is appropriately

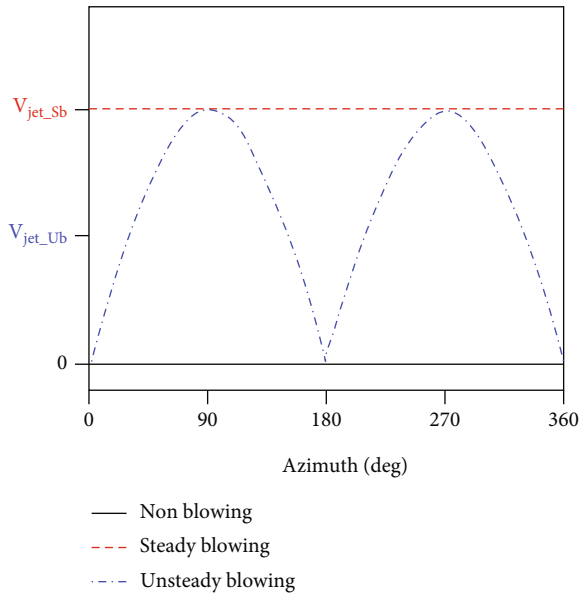

Figure 3: Jet velocity variation in the unsteady blowing case.

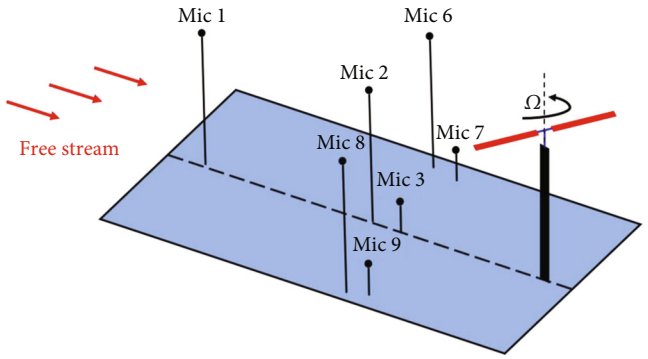

Figure 4: Microphone locations in the OLS rotor noise experiment [20, 21, 33].

Table 1: Coordinates of microphone locations (normalized by the rotor chord length) [20, 21, 33].

Microphone	x	y	z
1	-63.43	0.0	0.0
2	-31.717	0.0	0.0
3	-27.467	15.858	0.0
6	-27.467	0.0	15.858
7	-23.787	15.858	13.733
8	-27.467	0.0	-15.858
9	-23.787	15.858	-13.733

Table 2: Comparison of the computational cost, thrust coefficient of three grid resolutions.

Blowing case	Grid case	CPUh/rev	Thrust coefficient
Nonblowing	Benchmark Grid	640.0	0.00539
	Finer Grid	1304.1	0.00541
	Coarser Grid	374.4	0.00538
Steady blowing	Benchmark Grid	654.1	0.00505
	Finer Grid	1359.7	0.00506
	Coarser Grid	411.5	0.00505
Unsteady blowing	Benchmark Grid	648.2	0.00521
	Finer Grid	1368.0	0.00522
	Coarser Grid	392.5	0.00520

Notes: Benchmark Grid (background grid points: $300 \times 166 \times 247$), Finer Grid (background grid points: $300 \times 331 \times 247$), and Coarser Grid (background grid points: $300 \times 83 \times 247$). The same blade grid of $225 \times 80 \times 155$ points used in the three cases.

simplified and modeled in the CFD method as the mass flow outlet boundary condition of the surface grids at the defined jet slot location on the blade surface. Figure 2 shows that the defined jet slot is located on a 15×5 (spanwise and streamwise) grid cell face near the trailing edge on the blade upper surface near the rotor tip in the blowing case. Admittedly, some practical problems related to surface blowing are ignored in the numerical modeling, such as how to generate air blowing on the blade surface. The source of compressed air may need to be supplied through a separate compressor or air pump, and the compressed air may be supplied to blow on the blade surface through the internal jet ducts inside the blade. In addition, for the concept of unsteady surface blowing, the piezoelectrically actuated servo valve proposed by Vasilescu and Dancila [23–25] may also be required to modulate the air by a specific frequency or waveform during the blowing cycle. In their series of studies [23–25], the concept of unsteady blowing was achieved by using a piezoelectrically actuated servo valve, which periodically controlled the blowing air mass flow rate through the variation of slot height during the rotor rotation. In this paper, we modify the velocity term of the flux in the URANS equations to account for the effect of jet blowing. By applying the blowing jet velocity varied with the azimuthal angle, the velocity of the jet slot on the surface grid is the vector sum of the blade rotation velocity and the blowing jet velocity. The mass flow outlet boundary condition is adopted for the blade surface grids at the defined jet slot location; of course, for the other blade surface grids, only the wall viscous no-slip boundary condition must be satisfied. The density of the jet flow is extrapolated by the adjacent inner cells of the flow field. The pressure is then computed by the normal momentum equation including the surface velocity.

The constant jet velocity in the steady blowing case is defined as V_{jet_Sb}, and the time-varying jet velocity in the unsteady blowing case is defined as V_{jet_Ub}. We assume that, compared with steady blowing, the jet velocity in the unsteady blowing presents a periodic variation relationship with the change of rotor rotation azimuthal angle ($\psi = \Omega t$). Figure 3 shows the results investigating the variation relationship similar to the sine function to ensure a positive jet

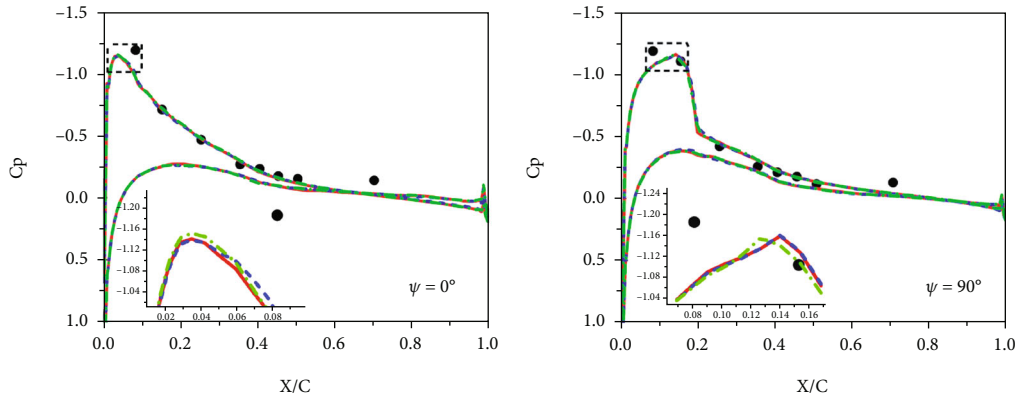

(a) Nonblowing

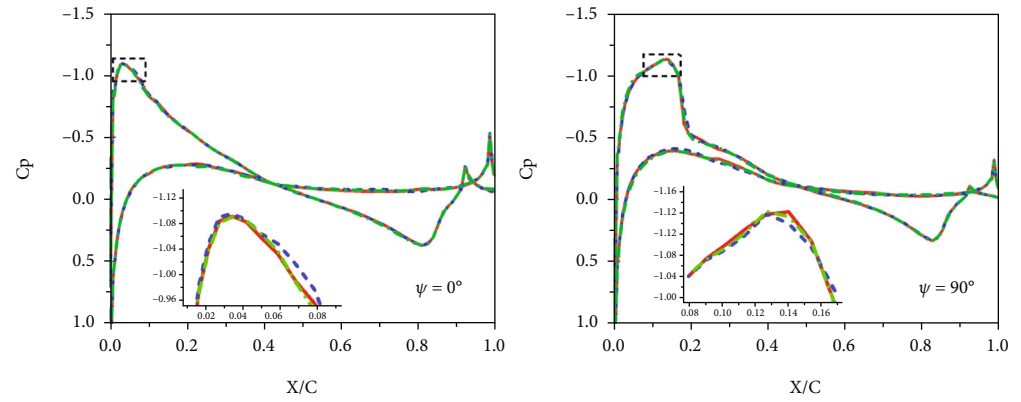

(b) Steady blowing

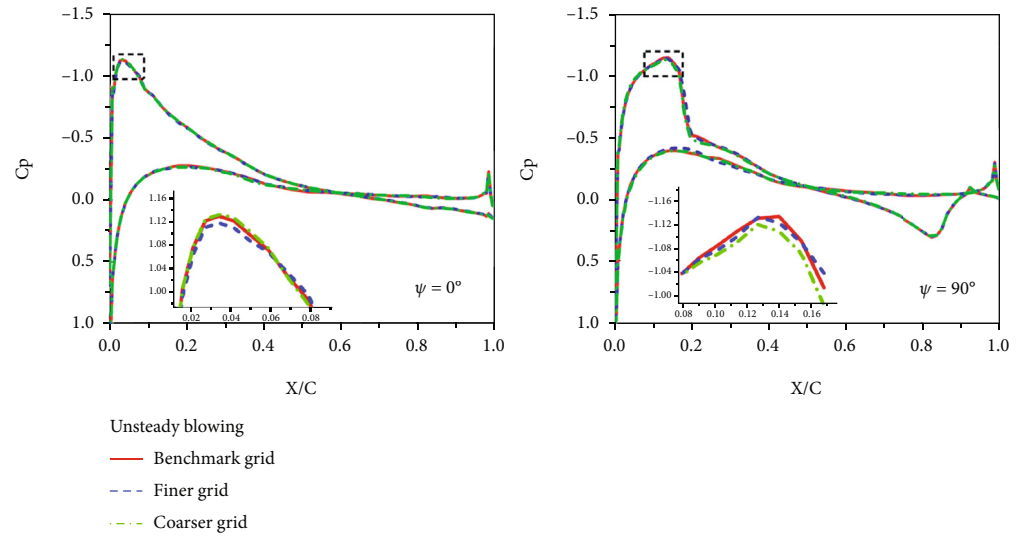

(c) Unsteady blowing

FIGURE 5: Blade surface pressure coefficients ($r/R = 0.955$) for the steady/unsteady blowing cases under the three background grid resolutions.

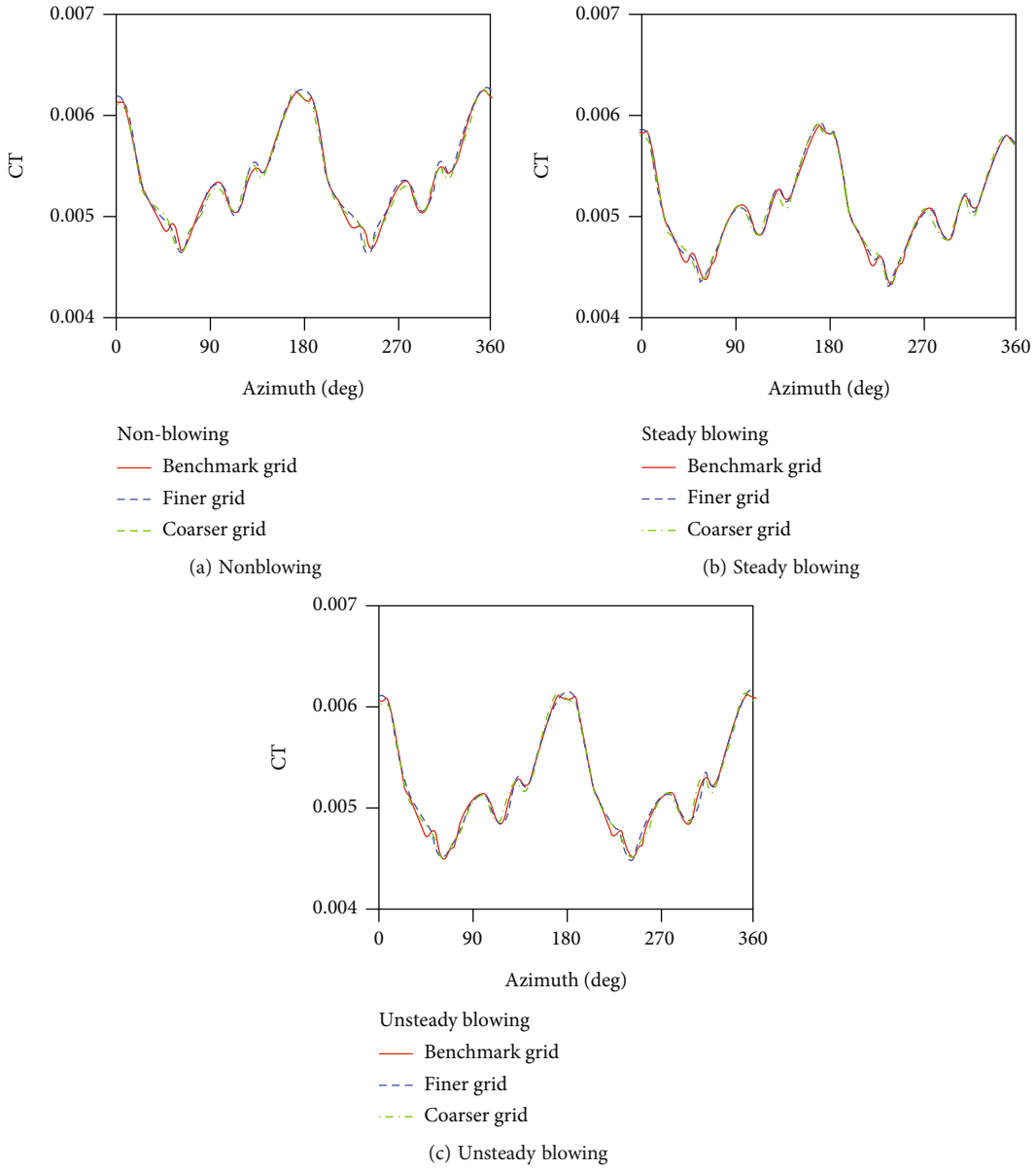

Figure 6: Rotor thrust coefficients with azimuthal angles for the steady/unsteady blowing cases under the three background grid resolutions.

velocity, that is,

$$V_{\text{jet\_Ub}} = V_{\text{jet\_Sb}}|\sin\psi| = V_{\text{jet\_Sb}}|\sin\Omega t|. \quad (1)$$

The mass flow rate of blowing can be computed by $\dot{m} = \rho V_{\text{jet}}\text{Area}_{\text{jet}}$, and the accumulated mass in t time is as follows:

$$m = \int_0^t \dot{m}dt = \int_0^t \rho V_{\text{jet}}\text{Area}_{\text{jet}}dt. \quad (2)$$

According to the jet velocity relationship between unsteady and steady blowing, it can be deduced that in the rotor rotation revolution, the ratio of the accumulated air mass cost of the unsteady blowing to the mass cost of steady blowing is as follows:

$$\frac{m_{\text{jet\_Ub}}}{m_{\text{jet\_Sb}}} = \frac{\int_0^T \rho V_{\text{jet\_Ub}}\text{Area}_{\text{jet}}dt}{\int_0^T \rho V_{\text{jet\_Sb}}\text{Area}_{\text{jet}}dt} = \frac{\int_0^{2\pi} V_{\text{jet\_Sb}}|\sin\psi|d\psi}{\int_0^{2\pi} V_{\text{jet\_Sb}}d\psi} = \frac{2}{\pi} = 63.7\%. \quad (3)$$

Thus, the mass required for unsteady blowing is 63.7% of that required for steady blowing per revolution. The other flow conditions of the unsteady blowing case are kept completely consistent with the nonblowing case and the steady blowing case, and simulations are carried out under the same solver settings and grid conditions.

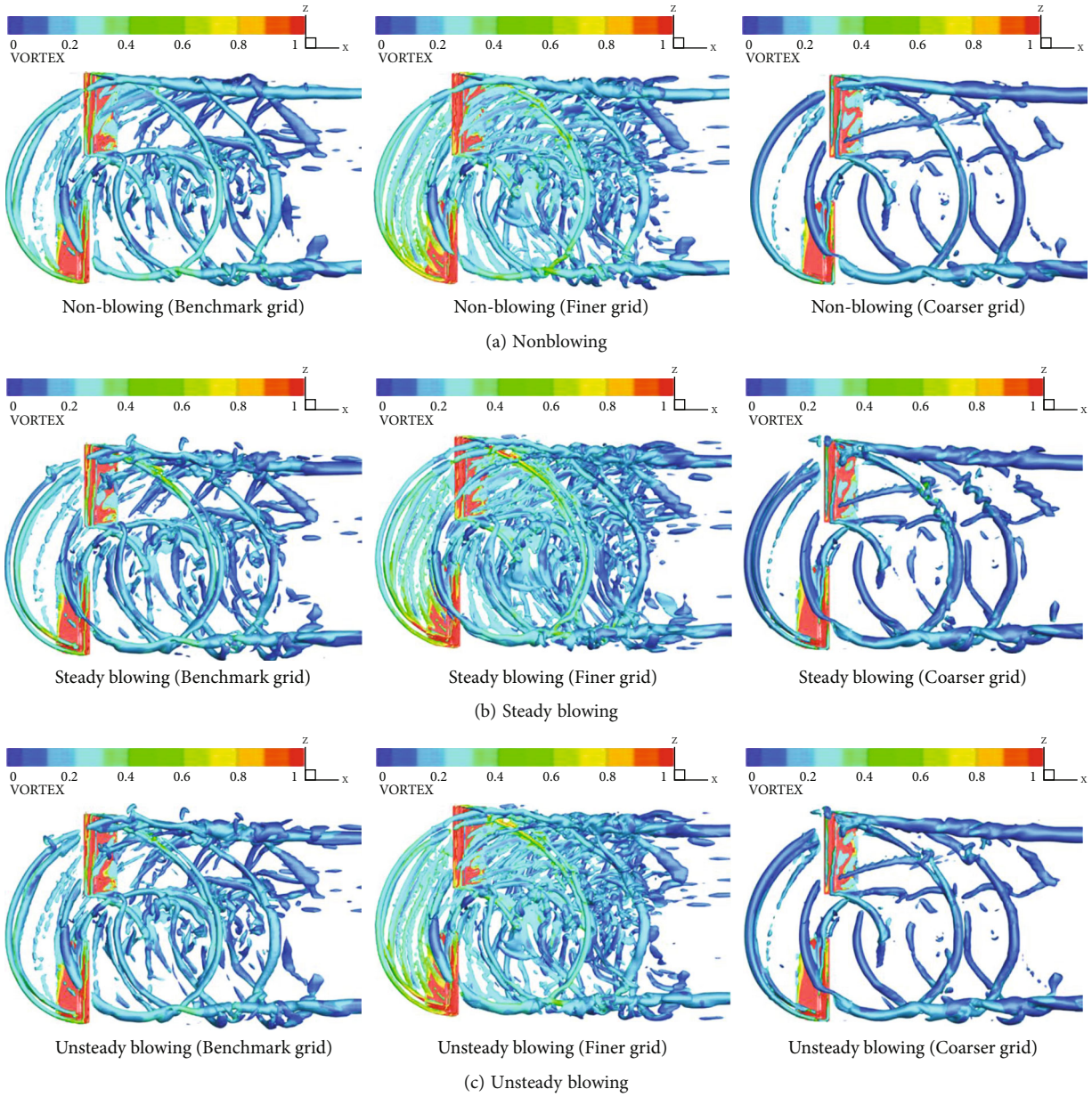

FIGURE 7: Rotor wake for the steady/unsteady blowing cases under the three background grid resolutions (isosurfaces of the Q criterion at $Q = 0.001$, colored by vorticity magnitude).

We have carried out detailed parametric studies on steady surface blowing in previous work [15], which discussed the effects of changes in parameters such as jet slot location, jet velocity, and jet slot area of steady blowing on the reduction of BVI noise. The BVI noise reduction results in this steady blowing research show that blowing near the trailing edge of the blade upper surface can effectively alter the tip vortex trajectory, increase the blade-vortex miss distance, and weaken the vortex strength, which is beneficial for reducing BVI noise. Moreover, the optimal jet velocity is 20% of the rotor tip speed. Compared with the nonblowing baseline case, the sound pressure level (SPL) can be reduced by up to 3.6 dB. However, this is obtained at the sacrifice of a 6.3% loss in the rotor thrust coefficient. The jet slot location we defined is located on the 15×5 (spanwise and streamwise) grid cell face near the trailing edge on the blade's upper surface. The length of the jet slot is spanwise 92–95% of the rotor radius, and the width is streamwise 84–90% of the chord length. The jet velocity is kept at 20% of the rotor tip speed, i.e., 45.2 m/s, the blowing direction is normal to the blade surface, and the air mass flow rate of the jet is 9.9×10^{-3} kg/s. The detailed results of the nonblowing baseline case and the $V_{\text{jet}} = 0.2V_{\text{tip}}$ steady blowing case were described in our previous work [15]. In the study of unsteady blowing, the defined slot location is the same as the jet slot location modeled in the steady blowing case. The maximum jet velocity of the unsteady blowing case is set to be 20% of the rotor tip velocity as the steady blowing

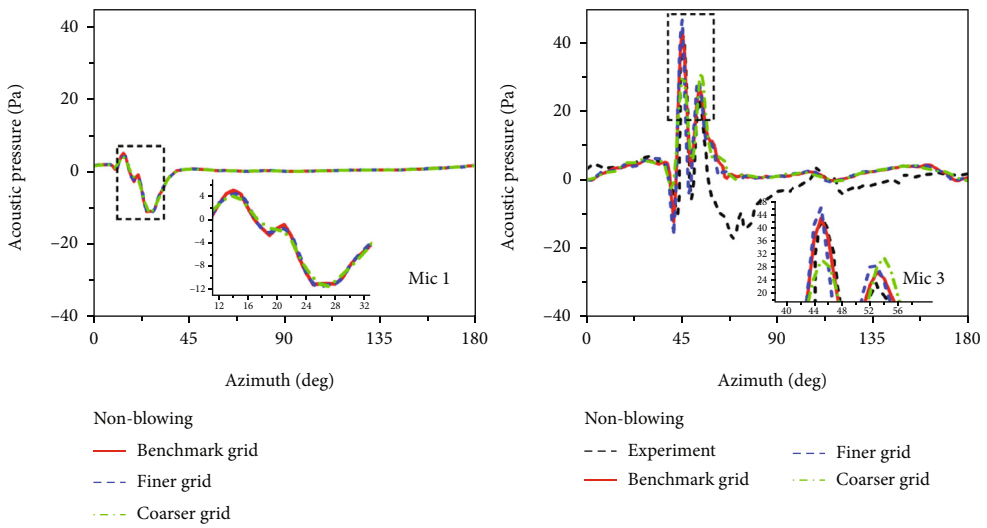

(a) Nonblowing

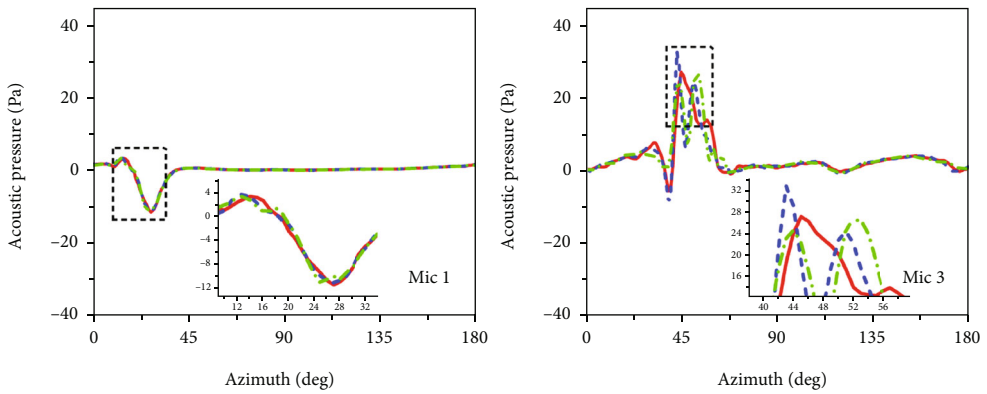

(b) Steady blowing

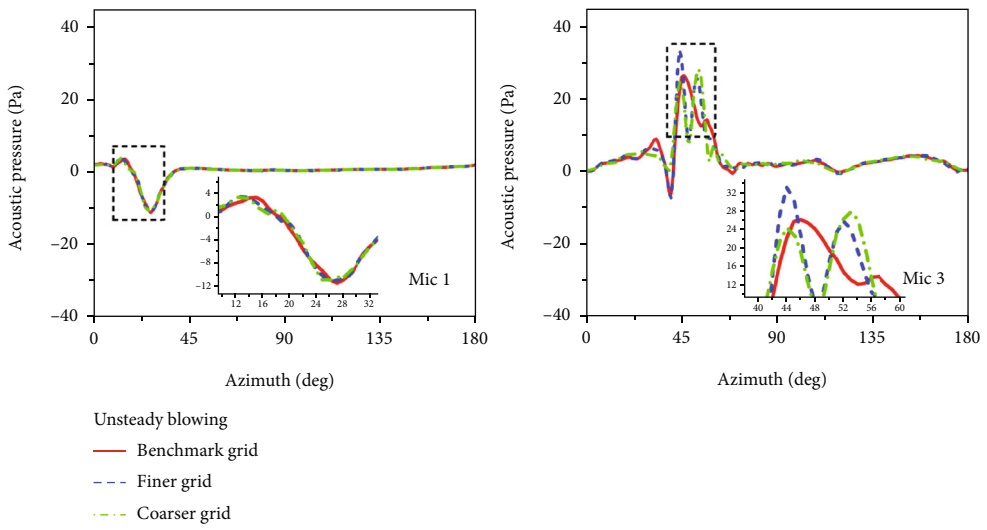

(c) Unsteady blowing

Figure 8: Acoustic pressure time history at microphones 1 and 3 for the steady/unsteady blowing cases under the three background grid resolutions.

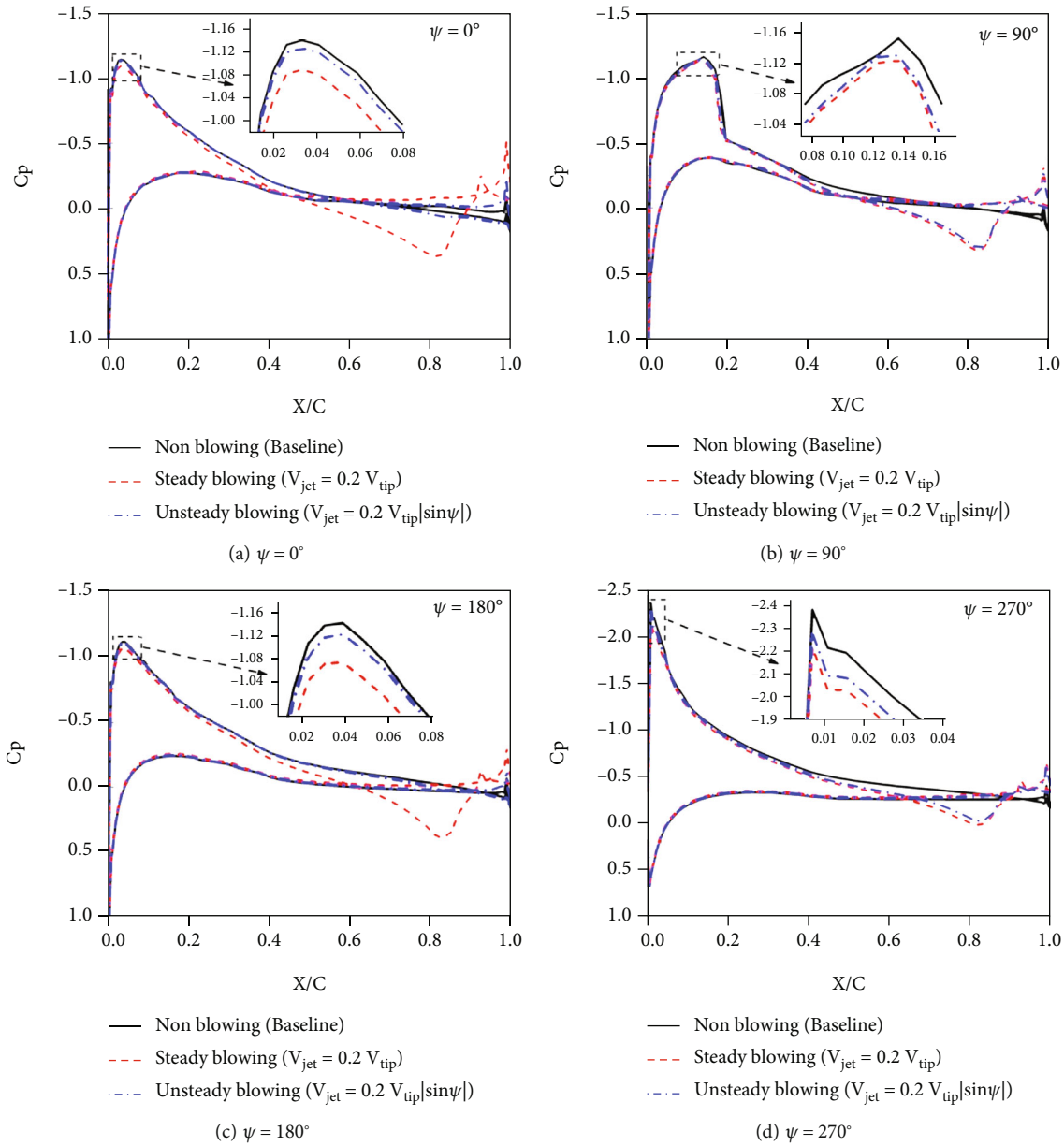

Figure 9: Blade surface pressure coefficients ($r/R = 0.955$) for the steady/unsteady blowing cases.

case; that is, the defined jet velocity varies with the azimuthal angle to satisfy $V_{jet} = 0.2V_{tip}|\sin\psi|$ during the rotor rotation revolution.

3. Results and Discussion

The 10014 test case under BVI state [32, 33] of the Operational Load Survey (OLS) rotor aerodynamic/noise experiment in the German-Dutch Wind Tunnel (DNW) is employed for the nonblowing case. The tested OLS rotor is a 1/7-scale model of the AH-1 helicopter main rotor. The rotor has two rectangular straight blades with a rotor radius of 0.958 m and a chord length of 0.1039 m and a negative blade twist of 8.2° from root to tip. The test condition configuration corresponds to a tip Mach number of 0.664, an advance ratio of 0.164, and a rotor thrust coefficient of 0.0054. The location of the microphones used to measure the acoustic signal in the experiment is shown in Figure 4 [20, 21, 33], where microphones 1, 2, 6, and 8 are installed in the plane of the rotor disk. Microphones 3, 7, and 9 are used to measure the BVI noise and are installed 3.44 R from the rotor hub 30° below the rotor plane, with the azimuthal angles of 180°, 150°, and 210°, respectively. The specific coordinates of all microphones [20, 21, 33] are listed in detail in Table 1 (normalized by chord length).

The flow solver is run for four revolutions with 1440 steps per revolution in the azimuthal direction during the CFD computation, that is, the time step corresponds to the 0.25° azimuthal angle. The CFD codes run on a standard PC with an 8-core Intel Core i7-7700 CPU (3.60 GHz) and

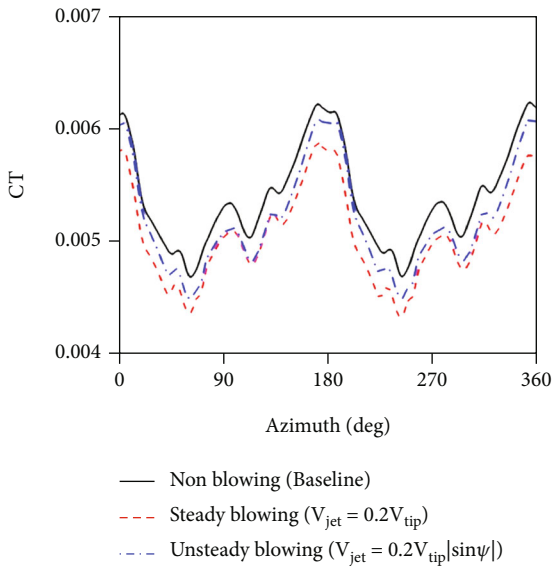

FIGURE 10: Rotor thrust coefficients with azimuthal angles for the steady/unsteady blowing cases.

32.0 GB of RAM [20, 21]. After the flow simulation is completed, the coordinates and the pressure of the blade surface grid output by the CFD codes are used as the input of the acoustic solver to predict the BVI noise.

3.1. Grid Convergence Study. We first conduct the grid convergence study using Benchmark Grid, Finer Grid, Coarser Grid described above for the nonblowing, steady, and unsteady blowing cases. Table 2 shows the comparisons of the computational cost and the computed rotor thrust coefficient of the three grid resolutions. The grid system of Benchmark Grid contains 17.9 million grid points. The grid systems of Finer Grid and Coarser Grid contain 30.1 million and 11.7 million grid points, respectively. The computational cost increases substantially as the grid resolution increases. The computational cost and the computed thrust coefficient of the blowing cases are very close under the three grid resolutions.

Figure 5 shows the comparisons of the surface pressure coefficients at the blade spanwise 0.955 R position at the azimuthal angles of 0° and 90° under the three background grid resolutions. The computed pressure coefficients of the three grid resolutions are relatively close, indicating that the background grid resolution has little effect on the pressure coefficient, and the computed results seem to be achieved the grid convergence. The results also show that for the calculation of blade surface pressure coefficient, using coarser background grid also has quite good accuracy. Similarly, Figure 6 also shows the grid convergence of the computed rotor thrust coefficient with azimuthal angles.

However, the background grid resolution has a great effect on the capture of the flow field details. Figure 7 shows the comparisons of the captured rotor wake for the three grid resolutions (Q criterion, $Q = 0.001$). It can be seen that compared with Coarser Grid, Benchmark Grid and Finer Grid can better predict the structure and trajectory of the tip vortex shedding from the blade. Benchmark Grid and Finer Grid have similar simulation resolutions in capturing the tip vortex structure, and the latter can capture more vortex sheets in the rotor disk than the former. Although Finer Grid exhibits the highest resolution for rotor wake simulation, its computational cost is extremely expensive (our CFD codes were run on the PC for more than 27 days to complete the case).

The convergence of noise prediction is analyzed by comparing the sound pressure time history at microphones 1 and 3. Figure 8 shows the computed acoustic pressure time history of microphones 1 and 3 for the three grid resolutions. For microphone 1 in the rotor plane, the thickness noise dominates the sound pressure waveform to show a negative peak. For microphone 3 below the rotor plane, the result exhibits the typical positive pulse characteristics of BVI noise by the vortex-induced load fluctuation. The background grid resolution has a great effect on the BVI noise prediction. The differences in the sound pressure positive peak of microphone 3 calculated by Coarser Grid are too large compared with Benchmark Grid and Finer Grid. The amplitudes and phases of BVI sound pressure in the nonblowing case computed by Benchmark Grid and Finer Grid are well resolved and are in good agreement with the experimental results. It is shown that the accurate prediction of BVI noise peak is closely related to the simulation resolution of rotor wake. The results calculated by Benchmark Grid and Finer Grid successfully capture the typical pulse fluctuation of the BVI noise at microphone 3, especially the peak sound pressure. However, the results also have large prediction deviation in some azimuthal phases. Although we have adopted the low numerical dissipation WENO scheme and the well-refined grid system, we only reduce the numerical dissipation in the simulated rotor wake. And the wake simulation is not only related to the discretization scheme and the grid refinement, but also to the accuracy of the turbulence model. To adopt a more advanced (e.g., two-equation) turbulence model will be a promising research direction in the future studies of rotor BVI. The results of the negative peak of microphone 1 and the positive peak of microphone 3 under the three grid resolutions are relatively close, showing a convergence trend. Due to the limited computational resources, considering that the accuracy of rotor wake simulation and noise prediction in Benchmark Grid is also quite good, the grid system of Benchmark Grid is used in the following section to study the flow control of unsteady surface blowing on rotor BVI.

3.2. Effect of Unsteady Blowing. In this section, a comprehensive numerical study is carried out to analyze the effects of steady/unsteady blowing on the aerodynamic force, flow field, and BVI noise compared with the nonblowing baseline case.

Figure 9 shows the comparisons of the pressure coefficients at the spanwise 0.955 R position of the blade in several azimuthal angles during the rotor rotation by the nonblowing baseline case and the steady/unsteady blowing cases. Compared with the baseline case, it can be observed that surface blowing has a significant effect on the pressure distribution near the trailing edge. The pressure coefficient

Table 3: Comparisons of the thrust coefficient and SPL for the baseline case and the steady/unsteady blowing cases.

Case	Thrust coefficient	SPL (dB)						
		Mic 1	2	3	6	7	8	9
Baseline	0.00539	101.622	107.506	110.326	107.701	106.535	104.680	110.373
Steady blowing	0.00505	**101.559**	**107.409**	**108.534**	107.754	106.790	**104.561**	**106.733**
Unsteady blowing	0.00521	**101.523**	**107.355**	**108.378**	107.787	106.596	**104.455**	**106.964**

Notes: The decrease in SPLs at the microphones compared with the baseline case is shown in bold.

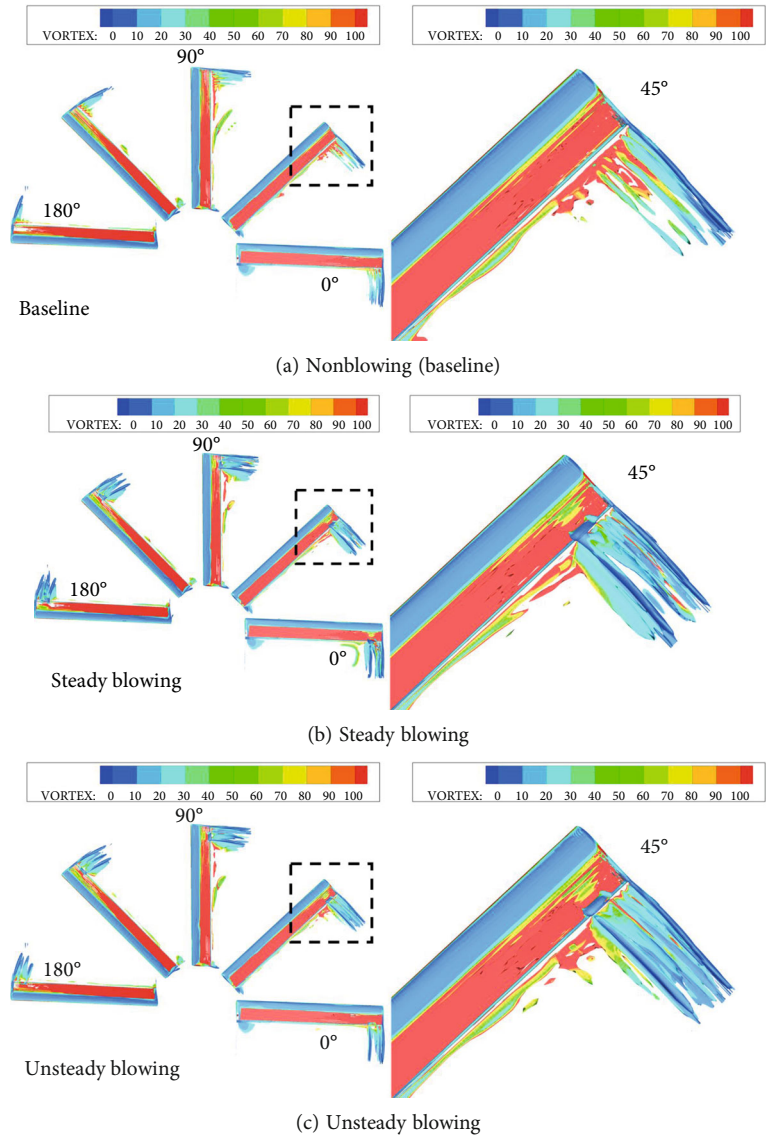

Figure 11: Near-body vortex structure from several azimuthal angles at the blade's advancing side for the steady/unsteady blowing cases (isosurfaces of the Q criterion at $Q = 1$, colored by vorticity magnitude).

changes dramatically near the trailing edge of the corresponding jet slot location, and the magnitude of the negative pressure peak near the leading edge is also slightly decreased. The envelope of the pressure coefficient of the unsteady blowing case is between the nonblowing baseline case and the steady blowing case. At the 0° and 180° azimuthal angles, the jet velocity of the unsteady blowing is 0, and the results of the surface pressure coefficient distribution are basically consistent with the baseline case; the jet velocity reaches the maximum at the azimuthal angles of 90° and 270°, which is equal to the jet velocity of steady blowing. Thus, the pressure coefficients are very close to the results of the steady blowing. Since the blowing direction is toward the upper surface, the surface blowing leads to rotor thrust loss. The

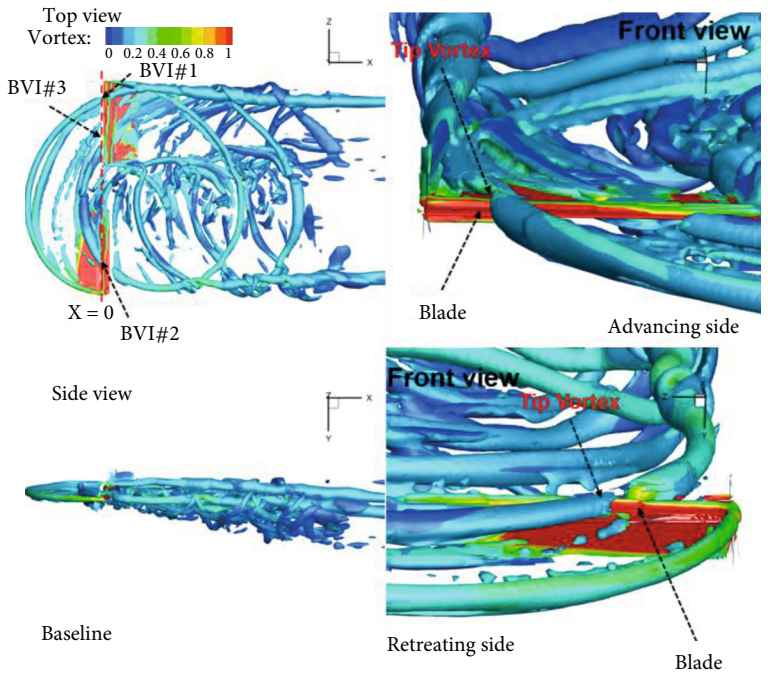

(a) Nonblowing (baseline)

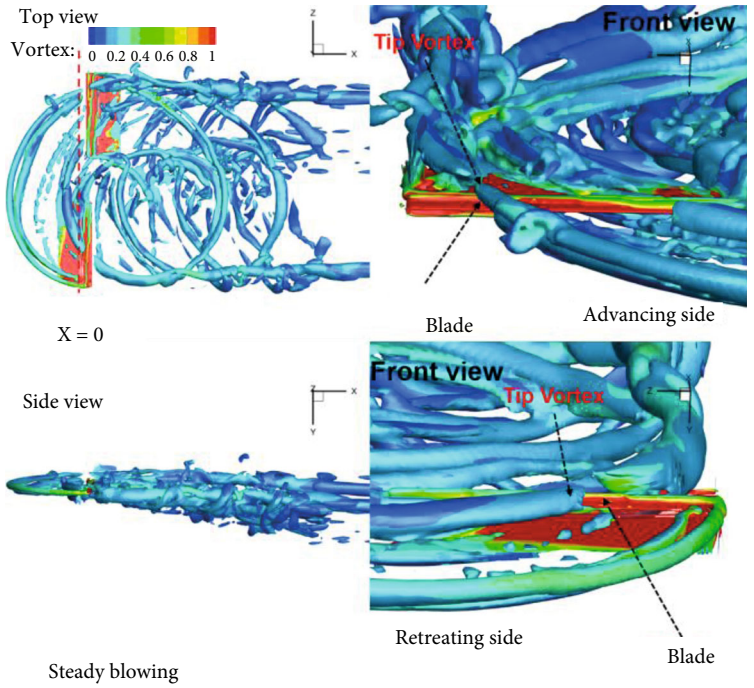

(b) Steady blowing

Figure 12: Continued.

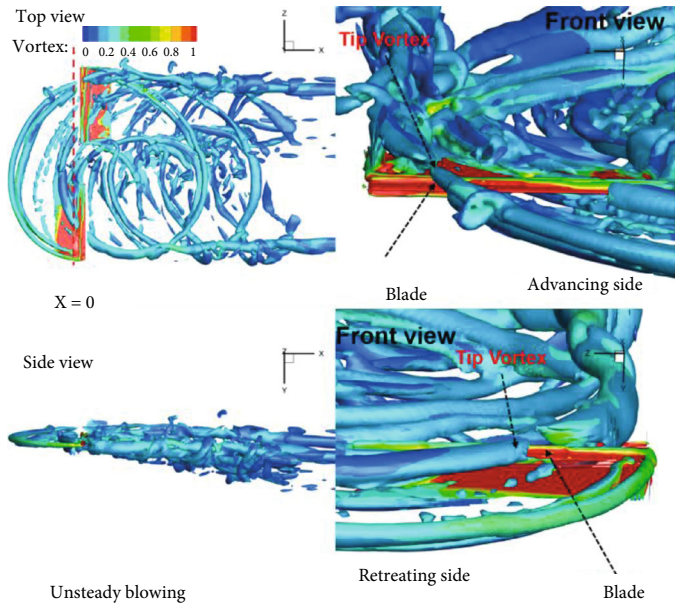

(c) Unsteady blowing

Figure 12: Vortex structure from several perspectives for the steady/unsteady blowing cases (isosurfaces of the Q criterion at $Q = 0.001$, colored by vorticity magnitude).

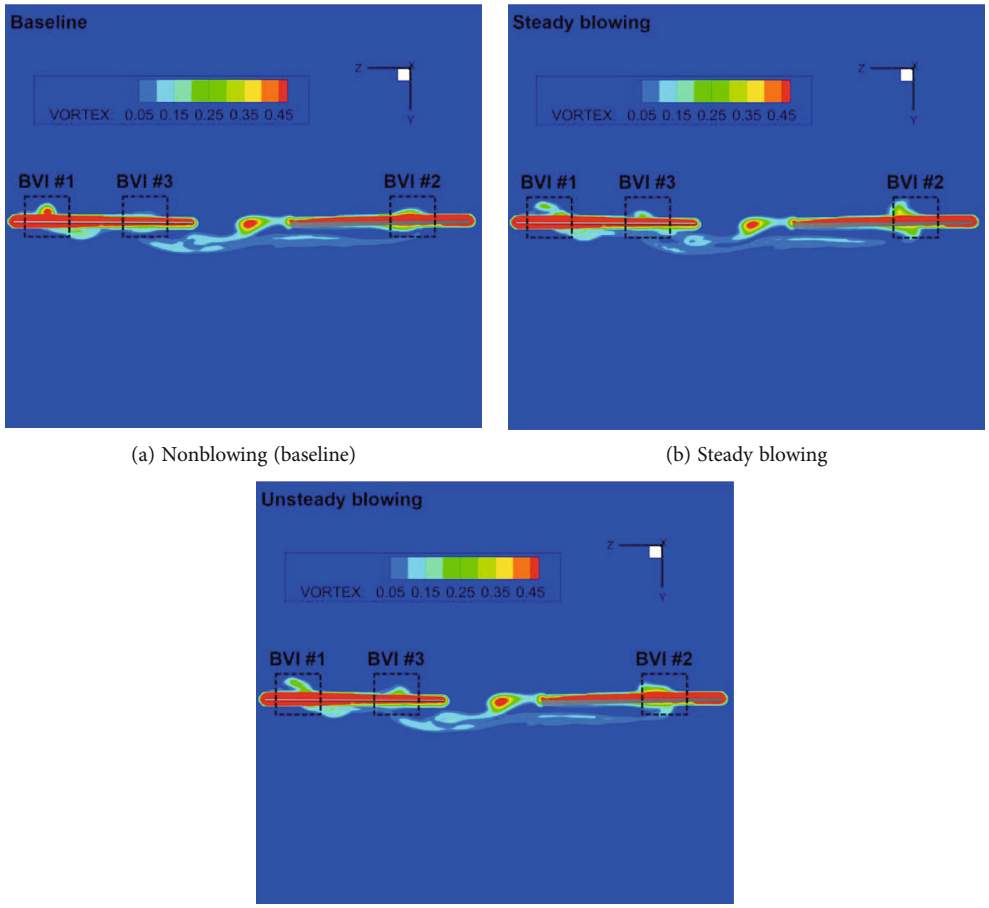

(a) Nonblowing (baseline)

(b) Steady blowing

(c) Unsteady blowing

Figure 13: Vorticity contours at the cutting plane of $X = 0$ at 90° azimuthal angle for the steady/unsteady blowing cases.

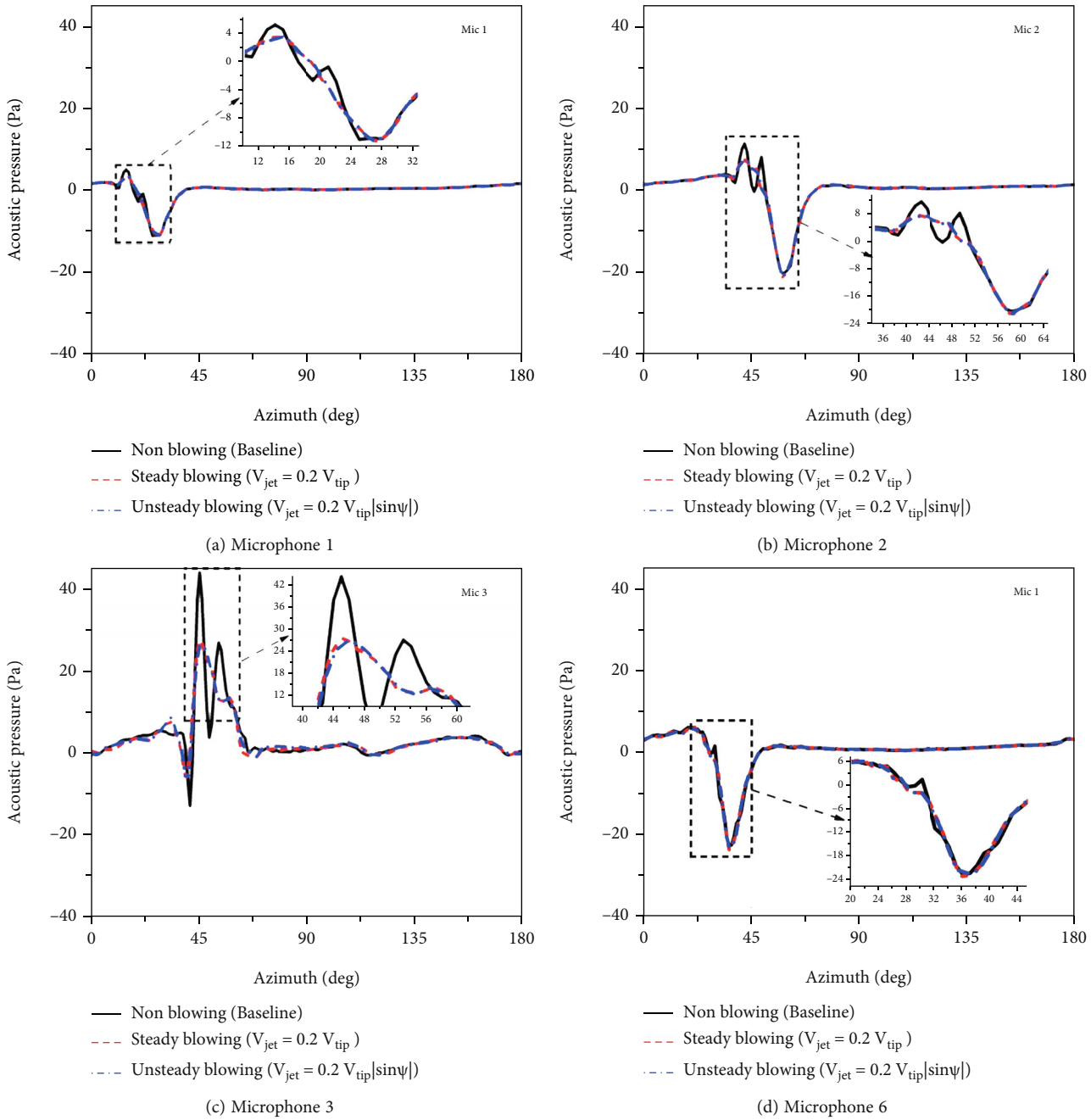

Figure 14: Continued.

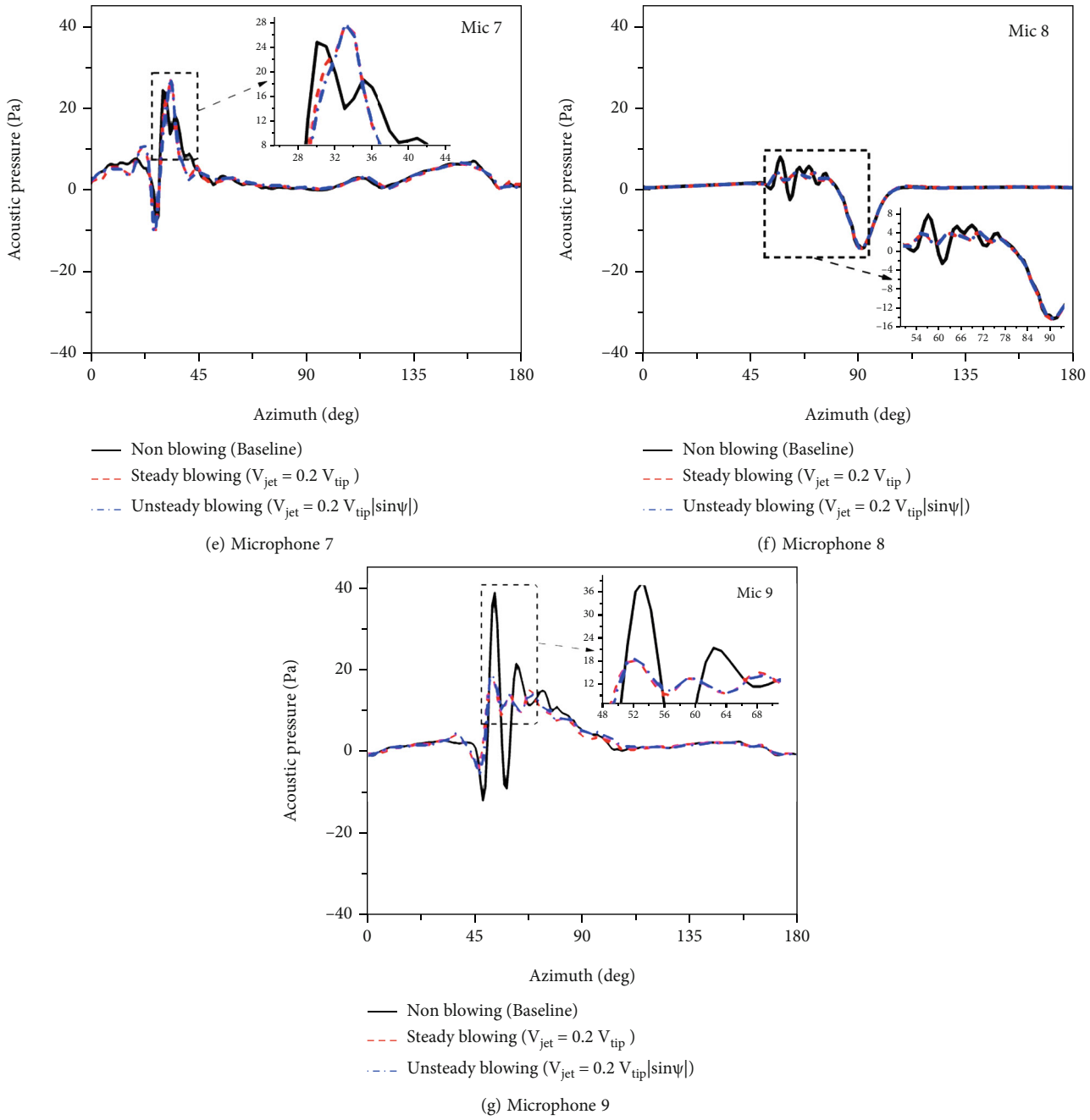

Figure 14: Acoustic pressure time history at all microphones for the steady/unsteady blowing cases.

jet velocity of unsteady blowing is always lower than that of steady blowing during the blowing cycle. According to the comparisons of the computed rotor thrust coefficient with azimuthal angles in Figure 10, the rotor thrust coefficient of the unsteady blowing case is always larger than that of the steady blowing case. Therefore, unsteady blowing causes less thrust loss than steady blowing. The results of the average thrust coefficient are listed in Table 3. Taking the rotor thrust coefficient of 0.00539 of the nonblowing baseline case as a reference, the rotor thrust coefficients of the steady and unsteady blowing cases are 0.00505 and 0.00521, respectively, which are decreased by 6.3% and 3.3%, respectively, compared with the baseline case.

Figure 11 shows the comparisons of the captured near-field vortex structure (Q criterion, $Q = 1$) from several azimuthal angles at the blade's advancing side for the baseline case and the steady/unsteady blowing cases. After introducing surface blowing, the jet blowing vertically upward from the blade surface, and an outward vortex forms behind the jet slot due to the interaction between the blowing jet and the free stream. The strength of the outward vortex is related to the mass flow rate of the blowing jet, and the vortex strength of steady blowing seems to be a little larger than that of unsteady blowing.

Figure 12 shows the comparisons of the captured vortex structure (Q criterion, $Q = 0.001$) from several perspectives

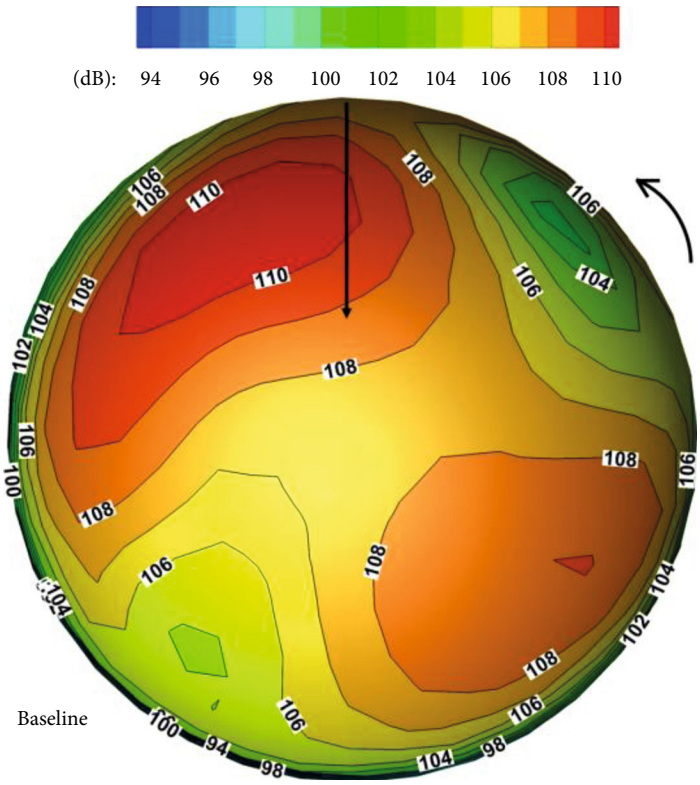

Baseline

(a) Baseline

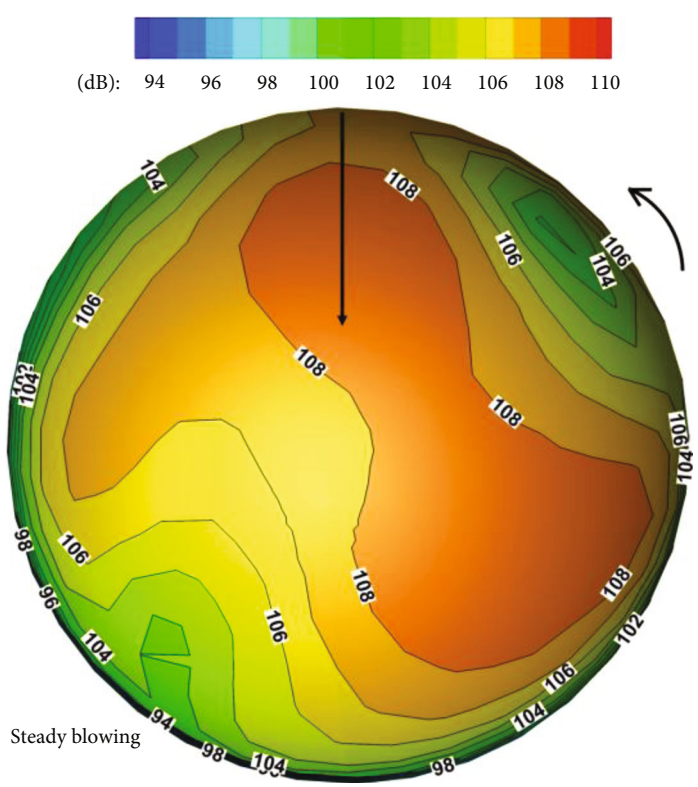

Steady blowing

(b) Steady blowing

Figure 15: Continued.

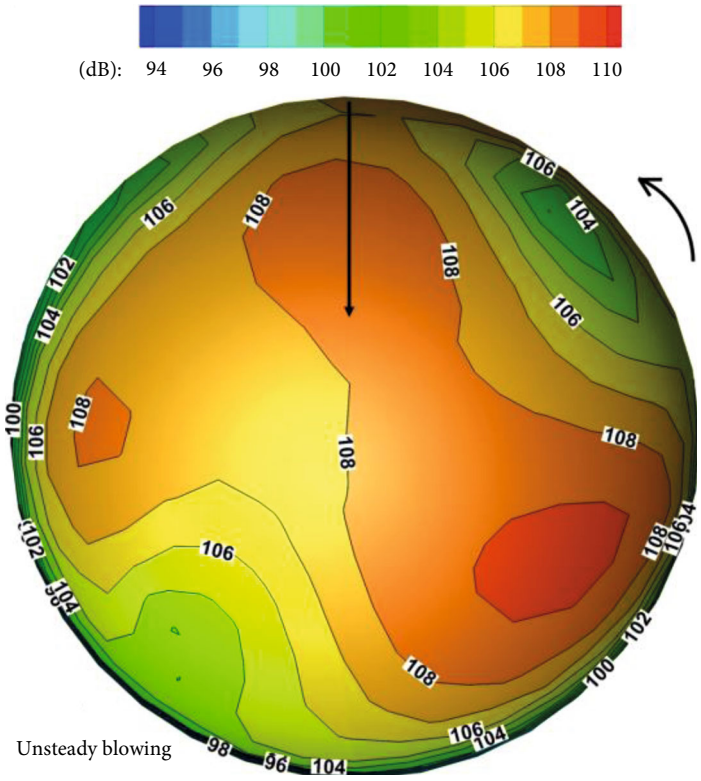

Unsteady blowing

(c) Unsteady blowing

Figure 15: SPL contours on a hemispherical surface (3.44 R from the rotor hub) for steady/unsteady blowing cases.

for the baseline case and the steady/unsteady blowing cases. The flow details of the BVI phenomenon are effectively resolved in the baseline case. The trajectory of the rolled-up tip vortex stays near the rotor disk. BVI occurs at the position where the tip vortex interacts with the blades in the rotor plane and then causes BVI noise. The top view shows the positions of the BVI. The #1 interaction position shows that the tip vortex shedding from the 270° azimuthal angle retreating side interacts with the 90° azimuthal angle advancing blade. The #2 position shows the interaction between the tip vortex shedding from the 90° azimuthal angle advancing side and the blade on the 270° azimuthal angle retreating side. The #3 shows the tip vortex shedding from the 90° azimuthal angle interacts with its own blade. In the two blowing cases, it can be seen that blowing induces the in-plane vortex to roll up and diffuse in the axial direction of the vortex motion. The enlarged front views, respectively, show the relative positions of the blade and tip vortices on the advancing and retreating sides. Compared with the baseline case, it can be clearly seen that the tip vortex is blown up, and the tip vortex trajectory is far away from the blade. Figure 13 shows the vorticity contours at the cutting plane of $X = 0$ at 90° azimuthal angle to describe the effects of blowing on the vortex strength. Compared with the BVI interaction positions of the section framed by the black line in the baseline case in Figure 13(a), the tip vortex strength of the surface blowing cases is decreased, and the vortex trajectory is also significantly altered. The blade-vortex miss distance is increased, so the surface blowing effectively weakens the BVI.

Figure 14 shows the comparisons of the predicted acoustic pressure time history at all microphones for the steady/unsteady blowing cases. The results of unsteady blowing are quite close to those of steady blowing. Similarly, for in-plane microphones 1, 2, 6, and 8, unsteady blowing has little effect on the change of sound pressure, while it significantly reduces the peak sound pressure at microphones 3 and 9. In Table 3, for the steady blowing case, the SPLs of microphones 3 and 9 are reduced by 1.8 and 3.6 dB, respectively, the SPL of microphone 7 is increased by 0.3 dB, and the rotor thrust coefficient shows a 6.3% loss compared with the baseline case. In contrast, the SPLs of microphones 3 and 9 for the unsteady blowing case are reduced by 1.9 and 3.4 dB, respectively, the SPL of microphone 7 is only increased by 0.1 dB, and the rotor thrust coefficient is decreased by 3.3%. Figure 15 further provides the comparisons of noise radiation distribution on the below plane hemispherical surface 3.44 R from the rotor hub. Surface blowing reduces the maximum SPL of BVI noise (more than 110 dB region) and changes the direction and distribution of the noise radiation. The changes in noise reduction and radiation of unsteady blowing are similar to those of steady blowing, and only a small region of the SPL distribution of the unsteady blowing is slightly larger than that of the steady

blowing. Compared with the steady blowing, the advantage of the unsteady blowing is mainly manifested in the less thrust loss. According to the noise results, the reduction in noise level caused by unsteady blowing is almost equivalent to that of steady blowing, but the loss in rotor thrust caused by unsteady blowing is only about half of that of steady blowing. Thus, active BVI control using the unsteady blowing method may have the potential to both minimize the thrust loss and effectively reduce BVI noise.

4. Conclusions

A numerical study on blade surface blowing control was carried out to reduce the rotor BVI noise by establishing an unsteady blowing model with time-varying jet velocity. Taking the OLS rotor BVI test case as the nonblowing baseline case, the effects and physics of steady/unsteady blowing on the rotor aerodynamics, flow field, and BVI noise were discussed, and the BVI noise reduction and thrust coefficient results of the two blowing methods were compared. The conclusions are as follows:

(1) The established CFD and noise numerical solver based on the URANS and FW-H method can effectively resolve the rotor flow field and BVI noise

(2) Surface blowing changes the tip vortex trajectory, increases the blade-vortex miss distance, reduces the vortex strength, and effectively weakens the BVI, thereby reducing the BVI noise. The SPL of the BVI noise using steady blowing can be reduced by 3.6 dB, with a 6.3% loss in the rotor thrust

(3) The accumulated air mass cost for unsteady blowing per rotation revolution is only 63.7% of that for steady blowing. From the noise reduction results, the level of noise reduction caused by unsteady blowing is almost similar to that caused by steady blowing (the SPL of BVI noise using unsteady blowing can be reduced by 3.4 dB), but the loss in the rotor thrust of the unsteady blowing is 3.3%, which is approximately half of that of steady blowing. Thus, BVI noise may be effectively reduced with lower cost and less thrust loss through unsteady surface blowing

(4) Motivated by the potential of unsteady blowing to reduce the rotor BVI noise, the authors intend to conduct more studies on unsteady blowing control. More diversified unsteady control methods should be investigated to obtain lower BVI noise and less thrust loss. Such studies will be continuous, with more methods investigated to realize the application of surface blowing in rotorcraft design

Data Availability

The data used to support the findings of this study are available from the corresponding author upon request.

Conflicts of Interest

The authors declare that they have no conflicts of interest.

Acknowledgments

This study was cosupported by the National Natural Science Foundation of China (grant number 11972190), A Project Funded by the Priority Academic Program Development of Jiangsu Higher Education Institutions (PAPD), and Postgraduate Research & Practice Innovation Program of Jiangsu Province (grant number KYCX19_0199).

References

[1] Y. H. Yu, B. Gmelin, W. Splettstoesser, J. J. Philippe, J. Prieur, and T. F. Brooks, "Reduction of helicopter blade-vortex interaction noise by active rotor control technology," *Progress in Aerospace Sciences*, vol. 33, no. 9-10, pp. 647–687, 1997.

[2] Y. H. Yu, "Rotor blade-vortex interaction noise," *Progress in Aerospace Sciences*, vol. 36, no. 2, pp. 97–115, 2000.

[3] G. Romani and D. Casalino, "Rotorcraft blade-vortex interaction noise prediction using the Lattice- Boltzmann method," *Aerospace Science and Technology*, vol. 88, pp. 147–157, 2019.

[4] P. Zehner, F. Falissard, and X. Gloerfelt, "Vortex model and blade span influence on orthogonal blade-vortex interaction noise," *AIAA Journal*, vol. 58, no. 8, pp. 3405–3413, 2020.

[5] Y. Liu and L. Tan, "Spatial–temporal evolution of tip leakage vortex in a mixed-flow pump with tip clearance," *Journal of Fluids Engineering*, vol. 141, no. 8, article 081302, 2019.

[6] Y. Liu and L. Tan, "Theoretical prediction model of tip leakage vortex in a mixed flow pump with tip clearance," *Journal of Fluids Engineering*, vol. 142, no. 2, article 021203, 2020.

[7] M. Liu, L. Tan, and S. Cao, "Method of dynamic mode decomposition and reconstruction with application to a three-stage multiphase pump," *Energy*, vol. 208, article 118343, 2020.

[8] Y. Han and L. Tan, "Dynamic mode decomposition and reconstruction of tip leakage vortex in a mixed flow pump as turbine at pump mode," *Renewable Energy*, vol. 155, pp. 725–734, 2020.

[9] K. Duraisamy, *Studies in Tip Vortex Formation, Evolution and Control*, Dissertation, University of Maryland, College Park, 2005.

[10] Z. Ye, F. Zhan, and G. Xu, "Numerical research on the unsteady evolution characteristics of blade tip vortex for helicopter rotor in forward flight," *International Journal of Aeronautical and Space Sciences*, vol. 21, no. 4, pp. 865–878, 2020.

[11] J. C. Hardin and S. L. Lamkin, "Concepts for reduction of blade/vortex interaction noise," *Journal of Aircraft*, vol. 24, no. 2, pp. 120–125, 1987.

[12] Y. O. Han and J. G. Leishman, "Investigation of helicopter rotor-blade-tip-vortex alleviation using a slotted tip," *AIAA Journal*, vol. 42, no. 3, pp. 524–535, 2004.

[13] R. P. White Jr., "Wind tunnel tests of a two bladed model rotor to evaluate the TAMI system in descending forward flight," 1977, *NASA CR-145195*.

[14] D. K. Gowanlock and C. S. Matthewson, "Control of rotor tip vortices," in *37th AIAA Aerospace Sciences Meeting and Exhibit*, Reno, NV, 1999.

[15] C. Weiland and P. P. Vlachos, "A mechanism for mitigation of blade–vortex interaction using leading edge blowing flow control," *Experiments in Fluids*, vol. 47, no. 3, pp. 411–426, 2009.

[16] A. A. Hassan, F. K. Straub, and B. D. Charles, "Effects of surface blowing/suction on the aerodynamics of helicopter rotor blade-vortex interactions (BVI) - a numerical simulation," in *52nd Annual Forum of the American Helicopter Society*, Washington, DC, 1996.

[17] Z. J. Liu, J. W. Russell, L. N. Sankar, and A. A. Hassan, "A study of rotor tip vortex structure alteration techniques," *Journal of Aircraft*, vol. 38, no. 3, pp. 473–477, 2001.

[18] K. Duraisamy and J. D. Baeder, "Numerical simulation of the effects of spanwise blowing on tip vortex formation," *Journal of Aircraft*, vol. 43, no. 4, pp. 996–1006, 2006.

[19] K. Duraisamy and J. D. Baeder, "Control of helicopter rotor tip vortex structure using blowing devices," in *60th Annual Forum of the American Helicopter Society*, Baltimore, MD, 2004.

[20] Y. Sun, G. H. Xu, and Y. J. Shi, "Numerical investigation on noise reduction of rotor blade-vortex interaction using blade surface jet blowing," *Aerospace Science and Technology*, vol. 116, article 106868, 2021.

[21] Y. Sun, G. H. Xu, and Y. J. Shi, "Parametric effect of blade surface blowing on the reduction of rotor blade–vortex interaction noise," *Journal of Aerospace Engineering*, vol. 35, no. 1, article 04021110, 2022.

[22] A. Brocklehurst and G. N. Barakos, "A review of helicopter rotor blade tip shapes," *Progress in Aerospace Sciences*, vol. 56, pp. 35–74, 2013.

[23] R. Vasilescu and D. S. Dancila, "Helicopter blade tip vortex modifications in hover using piezoelectrically modulated blowing," in *60th Annual Forum of the American Helicopter Society*, Baltimore, MD, 2004.

[24] R. Vasilescu and D. S. Dancila, "Rotor wake modifications in hover using unsteady spanwise blowing," in *44th AIAA Aerospace Sciences Meeting and Exhibit*, Reno, NV, 2006.

[25] R. Vasilescu and D. S. Dancila, "Electromechanical modeling of a piezoelectric actuator for modulated/vectored blowing," in *44th AIAA/ASME/ASCE/AHS Structures, Structural Dynamics, and Materials Conference*, Norfolk, VA, 2003.

[26] Z. Ye, G. H. Xu, and Y. J. Shi, "High-resolution simulation and parametric research on helicopter rotor vortex flowfield with TAMI control in hover," *Proceedings of the Institution of Mechanical Engineers, Part G: Journal of Aerospace Engineering*, vol. 232, no. 13, pp. 2513–2526, 2018.

[27] H. T. Qi, G. H. Xu, C. L. Lu, and Y. J. Shi, "A study of coaxial rotor aerodynamic interaction mechanism in hover with high-efficient trim model," *Aerospace Science and Technology*, vol. 84, pp. 1116–1130, 2019.

[28] R. Borges, M. Carmona, B. Costa, and W. S. Don, "An improved weighted essentially non-oscillatory scheme for hyperbolic conservation laws," *Journal of Computational Physics*, vol. 227, no. 6, pp. 3191–3211, 2008.

[29] Y. J. Shi, Q. J. Zhao, and G. H. Xu, "An analytical study of parametric effects on rotor-vortex interaction noise," *Proceedings of the Institution of Mechanical Engineers, Part G: Journal of Aerospace Engineering*, vol. 225, no. 3, pp. 259–268, 2011.

[30] F. Farassat, "Linear acoustic formulas for calculation of rotating blade noise," *AIAA Journal*, vol. 19, no. 9, pp. 1122–1130, 1981.

[31] K. S. Brentner and F. Farassat, "Modeling aerodynamically generated sound of helicopter rotors," *Progress in Aerospace Sciences*, vol. 39, no. 2-3, pp. 83–120, 2003.

[32] Y. H. Yu, C. Tung, J. Gallman et al., "Aerodynamics and acoustics of rotor blade-vortex interactions," *Journal of Aircraft*, vol. 32, no. 5, pp. 970–977, 1995.

[33] R. C. Strawn, E. P. N. Duque, and J. Ahmad, "Rotorcraft aeroacoustics computations with overset-grid CFD methods," in *54th Annual Forum of the American Helicopter Society*, Washington, DC, 1998.